Microstructural Evolution and Mechanical Properties of Y Added CoCrFeNi High-entropy Alloys Produced by Arc-melting

Gokhan Polat[1]* 🔘 **Hasan Kotan[2]** 🔘
ℝ[1]Izmir Katip Celebi University, Metallurgical and Materials Engineering, Izmir, Türkiye
ℝ[2]Bursa Technical University, Metallurgical and Materials Engineering, Bursa, Türkiye

ABSTRACT

The CoCrFeNi high entropy alloy (HEA) with face-centered cubic (FCC) crystal structure exhibits excellent ductility values even at cryogenic temperatures. However, since this HEA is relatively weak in strength, it may not meet the requirements of industrial applications in terms of strength-ductility trade-off. Therefore, the systematic addition of yttrium (Y) into CoCrFeNi HEA was investigated in the present study to increase the strength by solid solution and second phase strengthening. The HEAs were produced by vacuum arc melting, suction casting, and subsequent homogenization at 1150 °C for 24 h. The structural development of the HEAs was investigated by using the X-ray diffraction (XRD) technique which revealed the formation of a solid solution phase and $CaCu_5$-type hexagonal structure (HS) second phase. The corresponding microstructure of the HEAs was examined under a scanning electron microscope (SEM) revealing the transformation of the microstructure from elongated grains to nearly equiaxed grains with the increase of Y content from 2 at. % to 4 at. %. The mechanical properties of the HEAs were investigated by using hardness and compression tests. The results exhibited a dramatic increase in the hardness from 143 (±2) HV to 335 (±7) HV and in the yield strength from 130 MPa to 1025 MPa with 4 at. % Y addition. Our study has revealed that the addition of rare earth Y element results in further development in the strength of the CoCrFeNi for potential engineering applications.

Keywords:
High entropy alloys; Strength; Rare earth addition; Second phase

INTRODUCTION

High entropy alloys (HEAs) are a novel class of emerging materials with great potential to be applied in a wide range of engineering applications due to their unique comprehensive properties and structures (1, 2). Differing from conventional alloys, HEAs usually contain five or more principal elements in equiatomic or near-equiatomic ratios which causes an increase in the mixing entropy (ΔS_{mix}) of the alloys (3). Accordingly, HEAs are more likely to form simple solid solution structures such as face-centered cubic (FCC), body-centered cubic (BCC), and hexagonal close-packed (HCP) because of the reduced Gibbs free energy (4–6).

FCC-type HEAs have received much attention as compared to conventional alloys due to their exceptional properties such as fracture toughness at cryogenic

temperatures (7), and remarkable ductility (8). The well-known equiatomic CoCrFeNi HEA with a single FCC crystal structure is the starting point of numerous studies in the field of alloy development. The reported yield strength and ultimate tensile strength of the as-cast CoCrFeNi HEA are 160 MPa and 718 MPa, respectively (9). In addition, this HEA shows an excellent elongation to failure of over 50 % suggesting outstanding uniform deformation along with high strain hardening ability (9). This feature provides a great base for further strengthening the ductile HEAs. However, recent research indicates that a HEA matrix alone, particularly the single-phase FCC structure, is insufficiently robust for engineering applications at ambient and increased temperatures (10). Thus, the development of the mechanical properties of single-phase FCC CoCrFeNi HEAs has received great attention over the past decade (11). The main strategies

to enhance the mechanical properties of the HEAs include severe plastic deformation (12), tuning the composition of the main alloy (13–15), solid solution hardening by the addition of solute atoms (16), and second-phase hardening (17–19). It is widely known that adding additional alloying elements, such as Al, Mn, and Cu at low concentrations to the base CoCrFeNi alloy destabilizes the single FCC phase and promotes phase (20, 21). For instance, Wang et al. (22) reported that the presence of Al in $Al_{0.3}$CoCrFeNi HEA produced by the magnetic levitation induction technique and subsequent annealing at 800 °C resulted in the formation of a B2 phase. The formation of the B2 phase in the FCC matrix caused outstanding mechanical properties of ~870 MPa yield strength and ~1060 MPa tensile strength as well as the ductility of ~26 %. In addition, Chen et al. (23) produced $(CoCrFeNi)_{100-x}(ZrC)_x$ (x = 0-8, at. %) HEAs by arc-melting and investigated the strengthening mechanisms. They showed that the amounts of Laves and ZrC phases were increased with the increasing amounts of Zr and C additions, resulting in an improvement of the yield strength from 154 MPa to 374 MPa owing to the second phase strengthening mechanism.

The rare earth (RE) elements, often known as "industrial vitamins" due to their exceptional physical and chemical qualities, play a significant role in enhancing the quality of products and raising manufacturing performance. Because of their beneficial effects on molten steel purification and inclusion modification, additions of RE elements into steels have been a popular strategy for tailoring microstructure and improving mechanical performance (24–26). In addition, Y addition caused a substantial increase in the hardness of Fe-Al and Ni-Al-based superalloys (27, 28).

Similarly, it is shown in the literature that the mechanical properties of the HEAs could be enhanced by the addition of RE elements such as Y and Zr. For instance, Polat et al. (18) produced 1 and 4 at. % Y added CoCrFeNi HEAs by mechanical alloying followed by annealing and investigated the mechanical properties. They showed that an increase in the Y content caused a dramatic rise in the hardness from 215 to 435 HV after annealing at 1100 °C. Similarly, Tekin et al. (17) studied the effect of 1 and 4 at. % Zr addition into CoCrFeNi HEAs by mechanical alloying and subsequent annealing at 1100 °C. They reported a systematic increase in the hardness from 315 to 347 HV with the addition of 1 and 4 at. % Zr, respectively. These results demonstrate that the mechanical properties of HEAs could be further enhanced by the addition of RE elements synthesized by mechanical alloying. However, an inspection of the literature shows a lack of studies that utilized RE elements to increase the mechanical properties of the CoCrFeNi HEAs by melting techniques.

Table 1. The nominal compositions of the base, 2Y, and 4Y HEAs.

HEA	Compositions (at. %)				
	Co	Cr	Fe	Ni	Y
Base	25	25	25	25	-
2Y	24.5	24.5	24.5	24.5	2
4Y	24	24	24	24	4

In the present study, CoCrFeNi, $(CoCrFeNi)_{98}Y_2$, $(CoCrFeNi)_{96}Y_4$ HEAs were produced by vacuum arc melting to investigate the development of the mechanical properties due to the solid solution strengthening of solute Y atoms in the FCC crystal structure and formation of second phases. The formations of the phases were investigated experimentally by XRD, SEM, and EDS analyses along with the mechanical properties and interpreted thermodynamically.

MATERIAL AND METHODS

The CoCrFeNi, $(CoCrFeNi)_{98}Y_2$, $(CoCrFeNi)_{96}Y_4$ HEAs with the nominal compositions provided in Table 1 were produced by vacuum arc melting technique under argon atmosphere. For convenience, they are referred to as base, 2Y, and 4Y, respectively. The elemental Co, Cr, Fe, Ni, and Y chunks, each with purities higher than 99.9 wt. % were used to obtain the metal mixtures based on the nominal compositions. A total of 3 grams of metal chunk mixtures for each composition were charged into Edmund Buhler MAM-1 copper hearth arc-melter to produce ingots. The HEA ingots were flipped and re-melted at least 3 times to achieve the chemical homogeneity in the microstructure. Finally, the alloys were suction cast into a water-cooled cylindrical copper mold with a diameter of 4 mm. The suction-casted HEAs were homogenized at 1150 °C for 24 h in a tube furnace with a controlled atmosphere.

The structural characterizations of the HEAs were conducted by using a Panalytical Empyrean X-ray diffractometer with Cu-Kα radiation source (λ=1.5406 Å). The X-ray diffraction (XRD) characterization was conducted with a scanning rate of 1°/min between 35-100° values.

The relative intensity ratio (RIR) method is used to determine the percentages of the hexagonal structure (HS) phases based on the XRD analyses as shown in the following equation (29, 30):

$$\frac{V_{FCC}}{V_{HS}} = \frac{I_{(hkl)FCC}}{I_{(hkl)HS}} \cdot \frac{R_{HS}}{R_{FCC}} \qquad (1)$$

where v and I are the volume fraction and intensity of the most intense (hkl) peak, respectively. R-value of any phase a is given by (29–31):

$$R_\alpha = \frac{M_{(hkl)\alpha} \cdot LP_{(hkl)\alpha} \cdot |F_{(hkl)\alpha}|^2}{V_\alpha^2} \qquad (2)$$

where M, LP, F, and V are the multiplicity factor, Lorentz-polarization factor, structure factor, and volume of the unit cell, respectively.

The HEAs were etched by using a fresh aqua regia solution (a mixture of nitric acid and hydrochloric acid with a molar ratio of 1:3) for 1-2 min. The microstructural characterization and energy dispersive spectroscopy (EDS) were performed by using Hitachi SU1510 scanning electron microscope (SEM) with the Oxford Instruments x-act detector.

Hardness tests were conducted to determine the relationship between microstructure and mechanical properties of the HEAs as a function of Y content. The micro Vickers tests were carried out on the cylindrical 4 mm HEAs by using a load of 4.903 N (0.5 kgf) and a dwell duration of 10 sec at room temperature. At least 5 measurements were taken from each sample and their average was used for the corresponding hardness values. The compression tests were performed at room temperature using an INSTRON 5582 universal testing machine with a 10-ton capacity at a strain rate of 10^{-4} s^{-1} according to ASTM E9-09 standard. The samples were prepared by adjusting their height to be 1.5-2 times the diameter. To ensure the reliability of the test results, three samples were tested for each sample set.

RESULTS AND DISCUSSION

Structural and Microstructural Evolution of the HEAs

Fig. 1 shows the XRD patterns of the HEAs after homogenization at 1150 °C for 24 h. It should be noted that the homogenization duration and temperature were determined based on previous studies and ~$0.7T_m$, respectively, where Tm represents the theoretical melting points of the HEAs calculated through thermo-physical calculations (32, 33). The FCC phase is present in all the alloys, as seen by the (111), (200), (220), and (311) reflections of the FCC crystal structure. The base HEA consists of only these reflections in the XRD pattern, while additional reflections corresponding to a simple hexagonal structure (HS) were detected with Y additions. The formation of the HS could be attributed to the reaction between Y and Ni to form a $CaCu_5$ type Ni-Y rich phase with the P6/mmm space group, which agrees well with the previous reports indicated by Zhang et al. (26) and Zhou et al. (34). Due to the limited solubility of Y in Ni with a value of 0.4 at. % cause the formation of intermetallic compounds instead of the solid solution formation (35). In addition, the large negative enthalpy of mixing (ΔH_{mix}) value of -31

Table 2. Enthalpy of mixing (ΔH_{mix}, kJ/mol) values for the atom pairs in the HEAs (38).

	Co	Cr	Fe	Ni	Y
Co	0	-4	-1	0	-22
Cr		0	-1	-7	11
Fe			0	-2	-1
Ni				0	-31
Y					0

kJ/mol for the Ni-Y pair (Table 2) triggers the reaction between these elements as compared to the remaining elements in the HEAs (18). Xu et al. (36) showed that ΔHmix plays a critical role in the formation of the solid solution or intermetallic phases. The large negative values of ΔH_{mix} cause the increase in the bonding strength between the element pairs owing to their proper chemical reaction (37).

The increasing Y content from 2 at. % to 4 at. % raised the peak intensities of the HS phase suggesting the increase in the HS phase. In addition, the increasing Y content caused a shift towards a lower angle, as can be seen clearly in (311) reflection (Fig. 1) of the FCC phase. The decrease in the angles of the peak positions could be attributed to the increase in the lattice parameter of the HEAs due to the increase in the atomic radius of Y. That is, the increasing dissolution of the Y element in the HEAs causes a lattice distortion in the HEAs as pointed out by Zhang et al. (26).

The SEM images of the 2Y and 4Y HEAs are provided in Fig. 2. As can be deduced from the figure, the increasing Y content changes the shape of the etched region from elongated grains to nearly equiaxed grains. That is, the further addition of the Y element from 2 at. % to 4 at. % into the HEA results in the dendritic microstructure due to the increasing segregation into interdendritic regions. The frontal segrega-
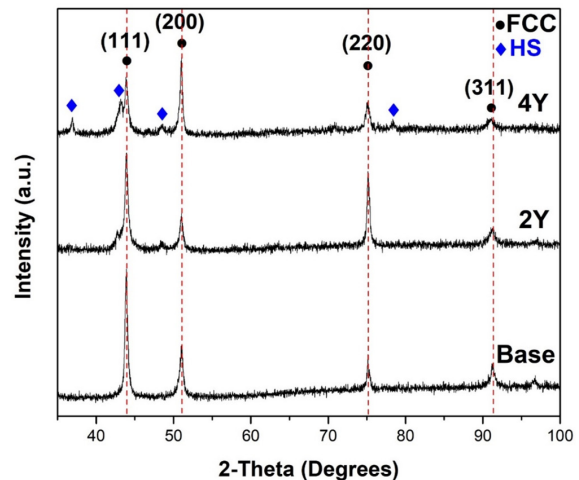

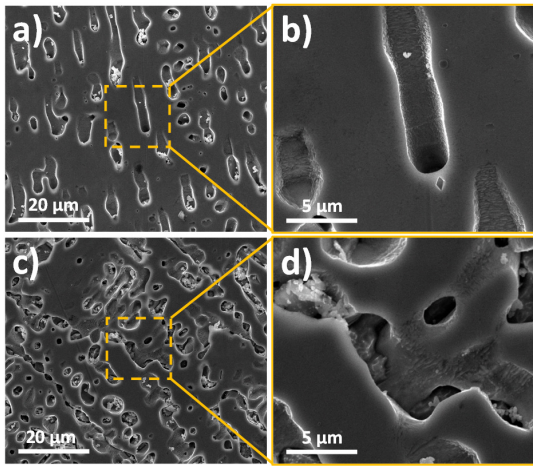**Figure 1.** XRD patterns of the base, 2Y, and 4Y HEAs.

Figure 2. SEM images of 2Y HEA a) low magnification, b) high magnification. SEM images of 4Y HEA a) low magnification, b) high magnification.
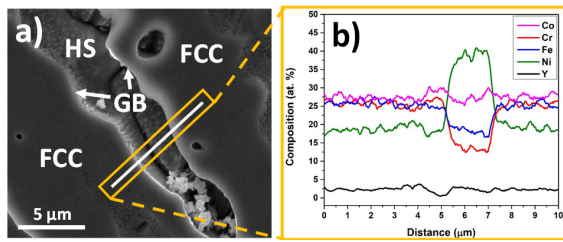

Figure 3. a) SEM image b) Corresponding EDS line scanning of etched 4Y HEA.

tion of the solute atoms in the solid-liquid interface causes a compositional change at the interface resulting in the formation of primary dendrites upon the solidification (39).

The SEM image and EDS line scanning provided in Fig. 3 show the compositional distribution between the matrix and second phase in the microstructure of the etched 4Y HEA. It should be noted that since the microstructure consists of dual phases of FCC and HS as shown with the XRD analyses (Fig. 1), the second phase could be indexed as HS. The EDS data provided in Fig. 3b shows that the FCC pha-

se is responsible for the almost homogeneously distributed areas of Co, Cr, and Fe with average values of around 27 at. %. In addition, the FCC matrix includes the homogeneously distributed Ni content with a value of ~17.5 at. %. This value is well below the nominal composition of the 4Y HEA having 24 at. % Ni in it. On the other hand, as can be seen in Fig. 3b, the Ni content reaches to a value of 40 at. % in the interdendritic regions, while the Co, Cr, and Fe elements deplete in this region. This suggests the segregation of the Ni element into the interdendritic region along with Y. In addition, the depletion of both Ni and Y elements could be seen in the grain boundary (GB) (Fig. 3a) of the FCC and HS phases.

It should be noted that although an increasing amount of Y could be expected in the interdendritic regions, the etching process decreases their amount. Therefore, detailed EDS analyses were conducted on the unetched 4Y HEA to reveal the exact elemental distribution of the FCC (matrix) and HS (segregated phase) as shown in Fig. 4. These results suggest the similar elemental distribution of Co, Cr, and Fe within the FCC matrix consistent with the EDS line scanning results. However, the compositions of Ni and Y elements in the HS phase reach values of 41.3 and 17.5 at. %, respectively, which is in line with the XRD results indicating the formation of the HS phase.

The Evolution of Mechanical Properties

The influence of the Y addition on the mechanical properties was investigated with the correlation of the HS phase formed in the microstructure. The hardness values and compression properties of the HEAs including yield stress ($\sigma_{0.2}$), fracture/peak stress (σ_p), and compressive strain to fracture (ε), are provided in Fig. 5 and summarized in Table 3. As seen in Fig. 5a, the amount of HS phase in the FCC matrix of the HEAs increased from 0 to 34 vol. % with the addition of 4 at. % Y, and the corresponding
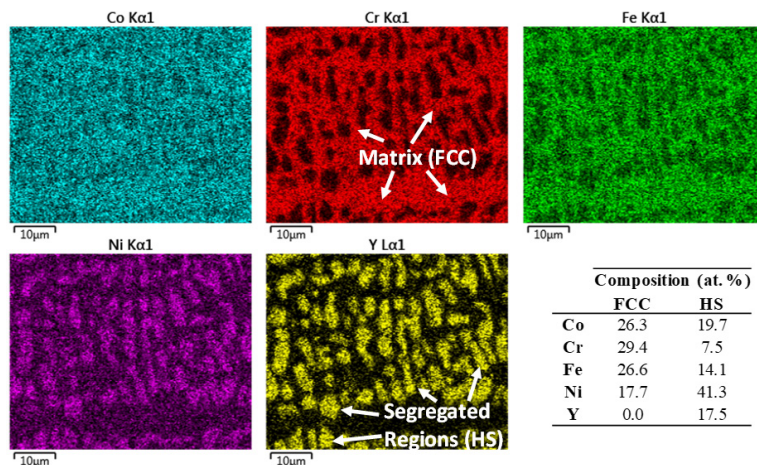

Figure 4. Mapping and point EDS analyses of unetched 4Y HEA.

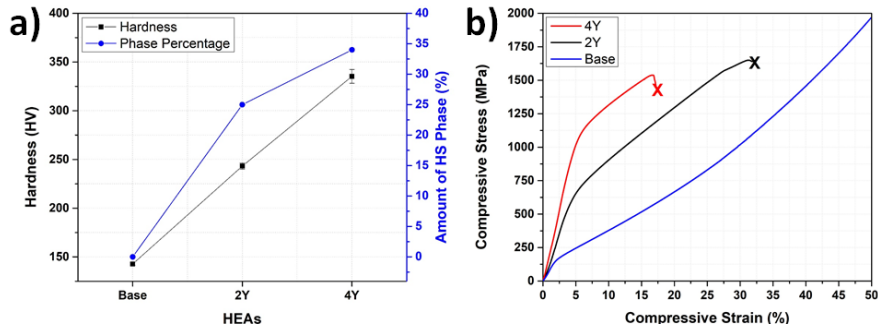|	Composition (at. %)	
	FCC	HS
Co	26.3	19.7
Cr	29.4	7.5
Fe	26.6	14.1
Ni	17.7	41.3
Y	0.0	17.5

Figure 5. a) Hardness and amount of the HS phase in the HEAs as a function of composition, b) Compressive stress-strain curves of the HEAs.
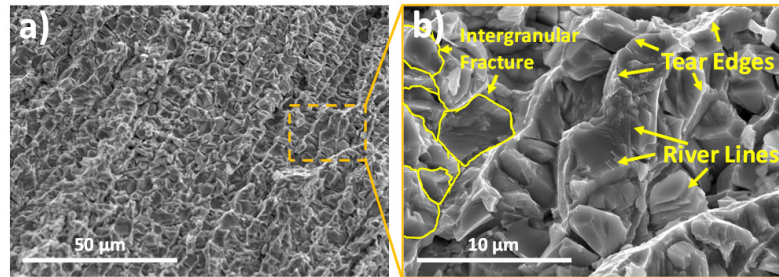

Figure 6. SEM images showing the fracture surface of the 4Y HEA after compression tests a) 1000x, b) 5000x.

hardness values were raised from 143 (±2) HV to 335 (±7) HV. In addition, the increasing Y content from 0 at. % to 4 at. % caused a dramatic increase in the yield strength from 130 MPa to 1025 MPa. On the other hand, the increase in the Y content from 2 at. % to 4 at. % decreased the compressive strain from 32 % to a value of around 16.5 %. It should be noted that the base HEA demonstrated high ductility and high strain hardening; its strength increased over 1960 MPa and it showed no signs of cracking up to compressive deformation of 50 %. Nevertheless, as can be deduced from the results, the formation of the HS phases plays a critical role in the improvement of the mechanical properties of the HEAs. These findings are in agreement with previous studies (26, 40, 41). The increased mechanical properties with the addition of alloying elements are generally divided into two categories; solid-solution strengthening and second-phase strengthening (14, 42, 43). Firstly, as explained in XRD analysis results (Fig. 1), the addition of Y causes a shift in the positions of the FCC reflections towards the lower angles due to the dissolution of Y in the matrix. This suggests a lattice distortion in the FCC crystal structure, and hence, an inc-

rease in the mechanical properties (44) due to the much larger atomic radius of Y as compared to the elements in the matrix (45). Secondly, the formation of the second phase causes a dramatic increase in the mechanical properties of the HEAs as reported in the previous studies (14, 32, 42). In the present study, the addition of excess Y into base HEA resulted in the formation of the HS phase in the microstructure. This causes an additional contribution to the increase of the mechanical properties due to the hard nature of the HS phase. The decrease in the available slip systems in the HS phases compared to the FCC results in the production of more brittle but stronger alloys (26). Therefore, the increasing amount of the HS phases up to 34 vol. % along with the solid solution strengthening has a vital contribution to the mechanical properties of the investigated HEAs.

The compression test results showed that Y addition caused the change in the failure mechanism of the HEAs. Therefore, the fracture morphology of the 4Y HEA was investigated under SEM to reveal the effect of Y on the fracture mode as shown in Fig. 6. As can be seen, although there are some river lines and smooth facets indicating the appearance of transgranular fractures, the intergranular dominated fracture was observed in the HEA due to the formation of hard and brittle HS phase in the intergrain regions resulting in the weakness of the intergrain regions (27, 46). In addition, the formation of tear edges in the fracture surface of the HEA shows relatively ductile behavior of the corresponding regions, which is consistent with what has been found in previous studies (32, 47). That is, combined with the above-mentioned results, it can be inferred that a

Table 3. Hardness and compressive properties of the base, 2Y and 4Y HEAs, and the amount of HS phase in the HEAs. *The base HEA demonstrated no fracture over the compressive strain value of 50 % and the compressive stress was continuously raised.

HEA	Amount of HS (%)	Hardness (HV)	$\sigma_{0.2}$ (MPa)	σ_p (MPa)	ε (%)
Base	0	143 (±2)	130	>1960*	>50*
2Y	25	243 (±3)	562	1650	31.5
4Y	34	335 (±7)	1025	1538	16.5

mixed mode of fracture indicating quasi-cleavage fracture was observed in 4Y HEA.

CONCLUSION

In the present study, The CoCrFeNi, $(CoCrFeNi)_{98}Y_2$, $(CoCrFeNi)_{96}Y_4$ HEAs were produced by vacuum arc melting and subsequent homogenization at 1150 °C for 24 h. The effect of Y addition on the structural, microstructural, and mechanical properties was investigated. The following conclusions could be drawn:

- The systematic addition of 2 at. and 4 at. % Y into CoCrFeNi HEA caused the dissolution of Y in the FCC crystal structure and the formation of $CaCu_5$-type HS second phase.

- The increasing Y content from 2 at. % to 4 at. % resulted in the transformation of the microstructure from an elongated shape to nearly equiaxed grains.

- The EDS analyses revealed the segregation of the Ni and Y atoms into intergrain regions.

- The hardness of CoCrFeNi HEA was increased from 143 (±2) HV to 335 (±7) HV with the addition of 4 at. % Y.

- The compressive yield strength, fracture stress, and strain of 1025 MPa, 1538 MPa, and 16.5 %, respectively, were achieved with the addition of 4 at. % Y.

- The strength-ductility trade-off of CoCrFeNi HEA could be enhanced by the addition of Y for the potential engineering application.

ACKNOWLEDGEMENT

CONFLICT OF INTEREST

The authors state that there is no conflict of interest.

AUTHOR CONTRIBUTION

Gokhan Polat: Methodology, Investigation, Data curation, Writing-review & editing.

Hasan Kotan: Data curation, Writing-review & editing.

References

1. Senkov ON, Miracle DB, Chaput KJ, Couzinie JP. Development and exploration of refractory high entropy alloys—A review. Journal of Materials Research 2018 33:19. 2018; 33: 3092–3128.

2. Zhang Y, Zuo TT, Tang Z, Gao MC, Dahmen KA, Liaw PK, Lu ZP. Microstructures and properties of high-entropy alloys. Progress in Materials Science. 2014; 61: 1–93.

3. Yeh JW, Chen SK, Lin SJ, Gan JY, Chin TS, Shun TT, Tsau CH, Chang SY. Nanostructured high-entropy alloys with multiple principal elements: Novel alloy design concepts and outcomes. Advanced Engineering Materials. 2004; 6: 299–303.

4. Guo S, Ng C, Lu J, Liu CT. Effect of valence electron concentration on stability of fcc or bcc phase in high entropy alloys. Journal of Applied Physics. 2011; 109: 103505.

5. 5. Ye YF, Wang Q, Lu J, Liu CT, Yang Y. High-entropy alloy: challenges and prospects. Materials Today. 2016; 19: 349–362.

6. Gao MC, Zhang B, Guo SM, Qiao JW, Hawk JA. High-Entropy Alloys in Hexagonal Close-Packed Structure. Metallurgical and Materials Transactions A: Physical Metallurgy and Materials Science. 2016; 47: 3322–3332.

7. Gludovatz B, Hohenwarter A, Catoor D, Chang EH, George EP, Ritchie RO. A fracture-resistant high-entropy alloy for cryogenic applications. Science. 2014; 345: 1153–1158.

8. Liu J, Guo X, Lin Q, He Z, An X, Li L, Liaw PK, Liao X, Yu L, Lin J, Xie L, Ren J, Zhang Y. Excellent ductility and serration feature of metastable CoCrFeNi high-entropy alloy at extremely low temperatures. Science China Materials. 2019; 62: 853–863.

9. Liu WH, Lu ZP, He JY, Luan JH, Wang ZJ, Liu B, Liu Y, Chen MW, Liu CT. Ductile CoCrFeNiMox high entropy alloys strengthened by hard intermetallic phases. Acta Materialia. 2016; 116: 332–342.

10. Yang T, Zhao Y, Liu W, Kai J, Liu C. L12-strengthened high-entropy alloys for advanced structural applications. Journal of Materials Research. 2018; 33: 2983–2997.

11. Liu WH, Yang T, Liu CT. Precipitation hardening in CoCrFeNi-based high entropy alloys. Materials Chemistry and Physics. 2018; 210: 2–11.

12. Gao X, Chen R, Liu T, Fang H, Wang L, Su Y. High deformation ability induced by phase transformation through adjusting Cr content in Co-Fe-Ni-Cr high entropy alloys. J Alloy Compd. 2022; 895: 162564.

13. Garcia Filho FDC, Ritchie RO, Meyers MA, Monteiro SN. Cantor-derived medium-entropy alloys: bridging the gap between traditional metallic and high-entropy alloys. Journal of Materials Research and Technology. 2022; 17: 1868–1895.

14. He MY, Shen YF, Jia N, Liaw PK. C and N doping in high-entropy alloys: A pathway to achieve desired strength-ductility synergy. Applied Materials Today. 2021; 25: 101162.

15. Zeng Z, Xiang M, Zhang D, Shi J, Wang W, Tang X, Tang W, Wang Y, Ma X, Chen Z, Ma W, Morita K. Mechanical properties of Cantor alloys driven by additional elements: a review. Journal of Materials Research and Technology. 2021; 15: 1920–1934.

16. Tong C-J, Chen Y-L, Yeh J-W, Lin S-J, Chen S-K, Shun T-T, Tsau C-H, Chang S-Y. Mechanical Performance of the AlxCoCrCuFeNi High-Entropy Alloy System with Multiprincipal Elements. Metallurgical and Materials Transactions A. 2005; 36: 881–893.

17. Tekin M, Polat G, Kotan H. An investigation of abnormal grain growth in Zr doped CoCrFeNi HEAs through in-situ formed oxide phases. Intermetallics. 2022; 146: 107588.

18. Polat G, Tekin M, Kotan H. Role of yttrium addition and annealing temperature on thermal stability and hardness of nanocrystalline CoCrFeNi high entropy alloy. Intermetallics. 2022; 146: 107589.

19. Tekin M, Polat G, Kalay YE, Kotan H. Grain size stabilization of oxide dispersion strengthened CoCrFeNi-Y2O3 high entropy alloys synthesized by mechanical alloying. Journal of Alloys and Compounds. 2021; 887: 161363.

20. Zhu ZG, Ma KH, Wang Q, Shek CH. Compositional dependence of phase formation and mechanical properties in three CoCrFeNi-(Mn/Al/Cu) high entropy alloys. Intermetallics. 2016; 79: 1–11.

21. Polat G, Atalay Kalsen TS. Al içeriğinin (CoCrFe)60AlXNi(40-X) yüksek entropili alaşımının yapısal ve mekanik özellikleri üzerindeki etkisi. Kahramanmaraş Sütçü İmam Üniversitesi Mühendislik Bilimleri Dergisi. 2023; 26: 812–822.

22. Wang X, Zhang Z, Wang Z, Ren X. Microstructural Evolution and Tensile Properties of Al0.3CoCrFeNi High-Entropy Alloy Associated with B2 Precipitates. Materials. 2022; 15: 1215.

23. Chen X, Qin G, Gao X, Chen R, Song Q, Cui H. Strengthening CoCrFeNi High Entropy Alloy by In-Situ Phases of Laves and ZrC. Metals and Materials International. 2023; 29: 1390–1398.

24. Wang LM, Lin Q, Yue LJ, Liu L, Guo F, Wang FM. Study of application of rare earth elements in advanced low alloy steels. Journal of Alloys and Compounds. 2008; 451: 534–537.

25. Zhao Y, Wang J, Zhou S, Wang X. Effects of rare earth addition on microstructure and mechanical properties of a Fe–15Mn–1.5Al–0.6C TWIP steel. Materials Science and Engineering: A. 2014; 608: 106–113.

26. Zhang LJ, Zhang MD, Zhou Z, Fan JT, Cui P, Yu PF, Jing Q, Ma MZ, Liaw PK, Li G, Liu RP. Effects of rare-earth element, Y, additions on the microstructure and mechanical properties of CoCrFeNi high entropy alloy. Materials Science and Engineering: A. 2018; 725: 437–446.

27. Atas MS, Yildirim M. Structural properties and cyclic oxidation behavior of Ni-Al-Y superalloys. Kovove Materialy. 2022; 60: 281–292.

28. Yildirim M, Atas MS, Akdeniz MV, Mekhrabov AO. Effect of Y Addition on the Structural Properties and Oxidation Behavior of Fe60Al40-nYn Alloys (n= 1, 3, and 5 at.%). Materials at High Temperatures. 2022; 39: 220–230.

29. Cullty B., Stock SR. Elements of X-Ray Diffraction: Third Edition. New York: Prentice-Hall, 2014.

30. John R, Karati A, Garlapati MM, Vaidya M, Bhattacharya R, Fabijanic D, Murty BS. Influence of mechanically activated annealing on phase evolution in Al0.3CoCrFeNi high-entropy alloy. Journal of Materials Science. 2019; 54: 14588–14598.

31. Keleş A, Cengız R, Yildirim M. Effect of Alloying Elements and Technological Parameters of Austempering on the Structure and Mechanical Properties of Ductile Cast Iron (ADI). Metal Science and Heat Treatment. 2023; 65: 191–199.

32. Polat G, Erdal ZA, Kalay YE. Design of Novel Non-equiatomic Cu-Ni-Al-Ti Composite Medium-Entropy Alloys. Journal of Materials Engineering and Performance. 2020; 29: 2898–2908.

33. Moghanni H, Dehghani K, Shafiei A. Effects of process parameters on microstructure and mechanical properties of Al0.5CoCrFeNi high entropy alloy thin sheets using pinless friction stir welding. Journal of Materials Research and Technology. 2022; 16: 1069–1089.

34. Zhou YX, Hu MY, Yan P, Shi X, Chong XY, Feng J. A first-principles calculation of structural, mechanical, thermodynamic and electronic properties of binary Ni-Y compounds. RSC Advances. 2018; 8: 41575–41586.

35. Beaudry B, Daane A. Yttrium-nickel system. Trans Met Soc AIME. 1960.

36. Xu XD, Guo S, Nieh TG, Liu CT, Hirata A, Chen MW. Effects of mixing enthalpy and cooling rate on phase formation of AlxCoCrCuFeNi high-entropy alloys. Materialia. 2019; 6: 100292.

37. Kukshal V, Patnaik A, Bhat IK. Effect of cobalt on microstructure and properties of AlCr1.5CuFeNi2Cox high-entropy alloys. Materials Research Express. 2018; 5: 046514.

38. Takeuchi A, Inoue A. Classification of Bulk Metallic Glasses by Atomic Size Difference, Heat of Mixing and Period of Constituent Elements and Its Application to Characterization of the Main Alloying Element. Materials Transactions. 2005; 46: 2817–2829.

39. Oliveira PHF, Mancilha PHS, Reyes RAV, de Gouveia GL, Bolfarini C, Spinelli JE, Coury FG. Influence of the cooling rate on the solidification path and microstructure of a AlCoCrFeNi2.1 alloy. Materials Characterization. 2023; 203: 113121.

40. Hong X, Hsueh CH. Effects of yttrium addition on microstructures and mechanical properties of CoCrNi medium entropy alloy. Intermetallics. 2022; 140: 107405.

41. Silveira RMS Da, Guimarães AV, De Melo CH, Ribeiro RM, Farina AB, Malet L, De Almeida LH, Araujo LS. Effect of yttrium addition on phase transformations in alloy 718. Journal of Materials Research and Technology. 2022; 18: 3283–3290.

42. Stepanov ND, Yurchenko NY, Tikhonovsky MA, Salishchev GA. Effect of carbon content and annealing on structure and hardness of the CoCrFeNiMn-based high entropy alloys. Journal of Alloys and Compounds. 2016; 687: 59–71.

43. Fleischer RL. Substitutional solution hardening. Acta Metallurgica. 1963; 11: 203–209.

44. Lin CM, Tsai HL. Evolution of microstructure, hardness, and corrosion properties of high-entropy Al0.5CoCrFeNi alloy. Intermetallics. 2011; 19: 288–294.

45. Lokman M, Ab A. Enhanced lattice distortion, yield strength, critical resolved shear stress, and improving mechanical properties of transition-metals doped CrCoNi medium entropy alloy. RSC Advances. 2021; 11: 23719–23724.

46. Zhang J, Chen S, Liu J, Qing Z, Wu Y. Microstructure and Mechanical Properties of Novel High-Strength, Low-Activation Wx(TaVZr)100−x (x = 5, 10, 15, 20, 25) Refractory High Entropy Alloys. Entropy 2022, Vol 24, Page 1342. 2022; 24: 1342.

47. Seifi M, Li D, Yong Z, Liaw PK, Lewandowski JJ. Fracture Toughness and Fatigue Crack Growth Behavior of As-Cast High-Entropy Alloys. Jom. 2015; 67: 2288–2295.